Draft version October 30, 2018
Typeset using LaTeX **twocolumn** style in AASTeX61

arXiv:1810.11508v1 [astro-ph.GA] 26 Oct 2018

COMPLETE IRAC MAPPING OF THE CFHTLS-DEEP, MUSYC AND NMBS-II FIELDS

Marianna Annunziatella,[1] Danilo Marchesini,[1] Mauro Stefanon,[2] Adam Muzzin,[3] Daniel Lange-Vagle,[1] Ryan Cybulski,[1] Ivo Labbe',[4] Erin Kado-Fong,[5] Rachel Bezanson,[6] Gabriel Brammer,[7] David Herrera,[8] Britt Lundgren,[9] Z. Cemile Marsan,[3] Mario Nonino,[10] Gregory Rudnick,[11] Paolo Saracco,[12] Tal Tomer,[13] Frank Valdes,[14] Remco F. J. van der Burg,[15] Pieter van Dokkum,[16] David Wake,[9] and Katherine E. Whitaker[17,18]

[1]*Physics Department, Tufts University, 574 Boston Ave., Medford, 02155, MA*
[2]*Leiden Observatory, Leiden University, PO Box 9513, NL-2300 RA, Leiden, The Netherlands*
[3]*Department of Physics and Astronomy, York University, 4700 Keele St., Toronto, Ontario, MJ3 1P3, Canada*
[4]*Centre for Astrophysics and SuperComputing, Swinburne, University of Technology, Hawthorn, Victoria, 3122, Australia*
[5]*Department of Astrophysical Sciences, Princeton University, Princeton, NJ 08544, USA*
[6]*Department of Physics and Astronomy and PITT PACC, University of Pittsburgh, Pittsburgh, PA 15260, USA*
[7]*Space Telescope Science Institute, 3700 San Martin Drive, Baltimore, MD 21218, USA*
[8]*National Optical Astronomy Observatory, 950 North Cherry Avenue, Tucson, AZ 85719, USA*
[9]*Department of Physics, University of North Carolina Asheville, One University Heights, Asheville, NC 28804, USA*
[10]*INAF-Osservatorio Astronomico di Trieste, via G. B. Tiepolo 11, 34131, Trieste, Italy*
[11]*Department of Physics and Astronomy, University of Kansas, 1251 Wescoe Hall Dr., Room 1082, Lawrence, KS, USA*
[12]*INAF-Osservatorio Astronomico di Brera, Via Brera 28, I-20121 Milano, Italy*
[13]*Department of Astronomy and Astrophysics, University of California, Santa Cruz, CA, USA*
[14]*National Optical Astronomy Observatory, 950 North Cherry A venue, Tucson, AZ 85719, USA*
[15]*European Southern Observatory, Karl-Schwarzschild-Str. 2, 85748, Garching, Germany*
[16]*Astronomy Department, Yale University, New Haven, CT 06511, USA*
[17]*Department of Physics, University of Connecticut, 2152 Hillside Road, Unit 3046, Storrs, CT 06269, USA*
[18]*Cosmic Dawn Center (DAWN), Niels Bohr Institute, University of Copenhagen / DTU-Space, Technical University of Denmark*

ABSTRACT

The IRAC mapping of the NMBS-II fields program is an imaging survey at 3.6 and 4.5μm with the Spitzer Infrared Array Camera (IRAC). The observations cover three Canada-France-Hawaii Telescope Legacy Survey Deep (CFHTLS-D) fields, including one also imaged by AEGIS, and two MUSYC fields. These are then combined with archival data from all previous programs into deep mosaics. The resulting imaging covers a combined area of about 3 deg^2, with at least ~2 hr integration time for each field. In this work, we present our data reduction techniques and document the resulting coverage maps at 3.6 and 4.5μm. All of the images are W-registered to the reference image, which is either the z-band stack image of the 25% best seeing images from the CFHTLS-D for CFHTLS-D1, CFHTLS-D3, and CFHTLS-D4, or the K-band images obtained at the Blanco 4-m telescope at CTIO for MUSYC1030 and MUSYC1255. We make all images and coverage maps described herein publicly available via the Spitzer Science Center.

Keywords: Data Analysis and Techniques

1. INTRODUCTION

One of the major unsolved issues in astrophysics is how galaxy buildup proceeded in the early Universe. Evolutionary models predict that different mechanisms can play a fundamental role for galaxy growth, such as galaxy mergers (e.g. Hopkins et al. 2006; Somerville et al. 2008) or cold gas accretion within gas-rich proto-disks (e.g. Dekel et al. 2009). Whatever the physical mechanisms dominating galaxy evolution might be, they must reproduce the observed distribution of baryons at high redshift, and connect it to the subsequent evolution of galaxies within dark matter halos. In this context, it becomes crucial to have accurate measurements of galaxy number densities and stellar-mass evolution over most of the cosmic history ($z < 3-4$). So far, important discrepancies still exist between predictions from theoretical models and observations of the number density of the most massive galaxies ($M_\star > 3\times10^{11}M_\odot$) at high redshifts (eg., Fontanot et al. 2009; Marchesini et al. 2009, 2010; Ilbert et al. 2013; Hirschmann et al. 2016). In fact, theoretical models still under-predict the observed number density of these galaxies, unless the model-predicted stellar mass functions (SMFs) are convolved with large errors in $M_\star$ (e.g., $\sim$ 0.25 − 0.3 dex at z=2-3, Marchesini et al. 2009, 2010; Ilbert et al. 2013; Muzzin et al. 2013a), arguably much larger than the typical random errors on $M_\star$ for massive (hence bright) galaxies. This disagreement at the very high-mass end has been recently confirmed by recent surveys, e.g. the NEWFIRM (NOAO Extremely Wide-Field Infrared Imager) Medium-Band Survey (NMBS) (Whitaker et al. 2011) and the UltraVISTA survey (Muzzin et al. 2013b; Hirschmann et al. 2016). NMBS is a moderately deep survey covering 0.45 deg^2 over two $30'\times30'$ fields within the Cosmic Evolution Survey (COSMOS; Scoville et al. 2007) and the All-Wavelength Extended Groth Strip International Survey (AEGIS; Davis et al. 2007), chosen to take advantage of the wealth of publicly available ancillary data over a broad wavelength range, from the X-ray to the radio. Thanks to the medium-band near-infrared (NIR) filters, NMBS provides precise z_{phot} ($\Delta z/(1+z)\approx0.02$) and well-sampled spectral energy distributions (SEDs) for thousands of K-selected galaxies at $z > 1.5$.

One of the most remarkable results from NMBS is the clear detection of the galaxy bi-modality in the galaxy population (quiescent vs. star-forming) out to $z\sim2.5$ (Brammer et al. 2009). The NMBS showed that nearly all galaxies with $\log(M/M_{star}) > 10.5$ have red rest-frame U−V colors up to $z = 2$. Despite similar U−V colors, the NMBS data showed that these galaxies have strikingly different properties, with approximately half being red due to a lack of recent star formation (quiescent), the other half being red due to vigorous dusty star formation. This result showed the limitations of using a single color to identify quiescent galaxies at $z > 1$. Instead, star-forming and quiescent galaxies can be robustly separated out to $z\sim3$ with a two-color criterion using the rest-frame U−V versus V−J diagram (UVJ diagram, hereafter). However, for high redshift galaxies, 3.6 and 4.5 μm imaging with IRAC (Fazio et al. 2004) aboard the Spitzer Space Telescope (Werner et al. 2004) are absolutely critical for the UVJ diagnostic, as the rest-frame V − J color cannot be directly measured without IRAC for galaxies at $0.8 < z < 3$. It is only thanks to IRAC in combination with the very precise photometric redshift (z_{phot}) from NMBS that the existence of the bi-modality and the existence of quiescent galaxies out to z$\sim$2.5 (and beyond) have been shown definitively (Whitaker et al. 2011). The lack of IRAC photometry prevents robust classification into quiescent and star-forming galaxies at $z > 0.8$.

While our knowledge of massive galaxies has grown significantly in the past years due to NMBS and other many NIR surveys, little is known about the evolution of the most massive galaxies (UMGs) with $M_\star > 3\times10^{11}M_\odot$. This is simply because their space density is extremely low ($\sim$30$\times$ lower than galaxies with $M_\star = 10^{11}M_\odot$). Even the largest NIR surveys have lacked the volume to detect them in significant numbers. Despite their rareness, these galaxies arguably represent the biggest problem in our understanding of how galaxies form. Abundance matching models suggest that ultra-massive galaxies, those with $M_\star = 3\times10^{11}M_\odot$ should reside in dark matter haloes of a few $\times10^{14}M_\odot$ at all redshifts, i.e., they are the progenitors of local Brightest Cluster Galaxies. While observationally the most massive galaxies appear to be the first to become quiescent, it is completely unknown why this is the case and what drives the quenching of the star formation.

In 2010-2012, NMBS-II (PI: Van Dokkum), a 44-night NOAO survey program with NEWFIRM was conducted with the primary goal of surveying a large enough volume to identify a statistically robust sample of UMGs out to $z = 3.5$. NMBS-II is shallower but 11$\times$ wider than NMBS, and it is unique for its combination of NIR medium-band imaging, well-sampled SEDs, and large area. NMBS-II covers a total of $\sim$ 5.4 deg^2 over 7 fields, namely CFHTLS-D1, CFHTLS-D2, (COSMOS), CFHTLS-D3, CFHTLS-D4, and 3 MUSYC (Multiwavelength Survey by Yale-Chile) fields, namely MUSYC1030, MUSYC1255 and MUSYC-ECDF. Observations of the NMBS-II are now completed, and multi-wavelength K-selected catalogs have been constructed (including deep optical ugriz data from the CFHTLS and U-V data from Galex). The NMBS-II J1J2J3H1H2K data, combined with deep optical data from the CFHTLS and IRAC imaging over the full survey area, promise to provide a mass-complete sample of $\sim$ 300 UMGs ($\log(M_\star/M_\odot) > 11.4$, of which ~50 with $\log(M_\star/M_\odot) > 11.6$) with high-confidence z_{phot} at $1.5 < z < 3$. This sample, spanning the full range of

star-formation activity, will provide the first comprehensive view of the population of UMGs at $z > 1.5$. This will be the largest sample of UMGs with accurate z_{phot} ever constructed. NMBS-II is truly unique as no other current survey has its combination of surveyed area and NIR medium-band coverage, preventing the delivery of sufficiently precise z_{phot} over a wide enough area to assemble similarly large samples of UMGs at $z > 1.5$.

However, Spitzer-IRAC coverage from previous programs of NMBS-II fields is available only for ~60% of the surveyed area, hence missing for $\sim 2.2\text{deg}^2$. IRAC data, besides being critical to classify the population of galaxies at z>0.8 into quiescent and star-forming galaxies using the UVJ diagram, are crucial for more accurate estimates of z_{phot} and $M_\star$, as well as for robust determinations of SFRs, as they significantly help breaking the age-dust degeneracy in the modeling of the SEDs.

With this paper, we present and publicly release the scientific mosaics, coverage maps, and 3σ depth maps at 3.6μm and 4.5μm for five of the NMBS-II fields. The mosaics combine both archival data and new data observed in Cycle 10. The paper is organized as follows. Section 2 describes all the programs that have been used to create single, contiguous deep images in the 3.6 and 4.5μm bands. In Section 3, we describe how the mosaics and coverage maps were produced, and Section 4 presents the characterization of the mosaics, including image quality and depth. All coordinates refer to the J2000 system. All magnitudes are in the AB system.

2. OBSERVATIONS

In this section, we present the NMBS-II fields and the individual Spitzer-IRAC programs that have been combined to produce deep IRAC mosaics over the NMBS-II, completing coverage of the full survey. Although the NMBS-II survey is comprised of seven fields, we produce IRAC mosaics only for five fields, because comprehensive IRAC mosaics in COSMOS and ECDFS are already publicly available from the Spitzer Science Center as part of previous IRAC surveys.

2.1. *NMBS-II Fields*

In this sub-section, we present the seven NMBS-II fields, including the ancillary data publicly available.

- CFHTLS-D1 (XMM-LSS) is a 1 deg^2 field centered on RA= 02:26:00.00 (hh:mm:ss) and DEC= -04:30:00.00 (dd:mm:ss). This field has ugriz imaging from the Canada-France-Hawaii Telescope Legacy Survey (CFHTLS). This field has NIR images in YJHK taken as part of the Visible and Infrared Survey Telescope for Astronomy (VISTA) Deep Extragalactic Observations (VIDEO) survey (Jarvis et al. 2013). Other NIR data are available through the WIRCam Infrared Deep Survey (WIRDS; Bielby et al. 2012). Imaging of the CFHTLS-D1 field at 250, 350, and 500 μm was provided by the Spectral and Photometric Imaging REceiver (SPIRE; Griffin et al. 2010) aboard the Herschel Space Observatory (Pilbratt et al. 2010), taken as part of the Herschel Multi-tiered Extragalactic Survey (HerMES; Oliver et al. 2012) X-ray observations of the CFHTLS-D1 field were taken from the X-ray Multi-mirror Mission space telescope (XMM-Newton; Jansen et al. 2001) as part of the XMM Medium Deep Survey (XMDS; Chiappetti et al. 2005). Spectroscopic data for this field have been acquired with the VIsible Multi-Object Spectrograph (VIMOS) as part of the VIMOS-VLT deep survey (VVDS). As a part of NMBS-II, this field was imaged in medium-bandwidth filters ($J_1J_2J_3H_1H_2$) over the wavelength range 1–1.8μm and in the K-band. CFHTLS-D1 has a 100% data coverage from the Spitzer Wide-area InfraRed Extragalactic Survey (SWIRE, Lonsdale et al. 2003). SWIRE is a wide-area, high galactic latitude imaging survey which covered roughly 50 deg^2 across a number of fields with the MIPS far-infrared camera and the with the IRAC mid-infrared camera.

- CFHTLS-D2 is a $2\,\text{deg}^2$ field centered on RA= 10:00:28.60 and DEC= 02:12:21.00. This field is part of the Cosmic Evolution Survey survey. (COSMOS; Scoville et al. 2007). Within COSMOS, $1\,\text{deg}^2$ has is also been imaged by CFHT as part of the Canada-France-Hawaii Telescope Legacy Survey Deep (CFHTLS-Deep). This field has X-ray imaging (Chandra and XMM, Elvis et al. 2009; Finoguenov et al. 2007, respectively) from COSMOS, HST imaging from the original COSMOS Hubble Space Telescope Treasury project, and from the Cosmic Assembly Near-infrared Deep Extragalactic Legacy Survey (CANDELS; Koekemoer et al. 2011), deep optical imaging taken with Hyper Suprime-Cam (HSC; Tanaka et al. 2017), and deep NIR imaging as part of UltraVISTA (McCracken et al. 2013) survey. As a part of NMBS-II, this field was imaged in medium-bandwidth filters ($J_1J_2J_3H_1H_2$), and in the K-band. Narrow-band NIR images of the COSMOS-HST field we also taken with Suprime-Cam on the Subaru Telescope within the Subaru COSMOS 20 project (Taniguchi et al. 2015). COSMOS has extensive spectroscopic data with over 97,000 spectra targeting over 68,000 unique objects. Major surveys include zCOSMOS (Lilly et al. 2007), and the VIMOS Ultra Deep Survey (VUDS; Le Fèvre et al. 2015). HST spectroscopy is also available from the 3D-HST program (van Dokkum et al. 2011). CFHTLS-D2 has 100% IRAC data coverage coming from multiple surveys, e.g. S-COSMOS (Sanders et al. 2007), the Spitzer

Extended Deep Survey (Ashby et al. 2013, SEDS;), S-CANDELS, (Ashby et al. 2015), Star Formation at 4 < z < 6 from the Spitzer Large Area Survey with Hyper-Suprime-Cam (SPLASH; Steinhardt et al. 2014), and Spitzer Matching survey of the UltraVISTA ultra-deep Stripes (SMUVS; Ashby et al. 2018).

- CFHTLS-D3 is a 1 deg^2 field centered on RA= 14:19:27.00 and DEC= +52:40:56.00. This field was imaged by CFHT both as part of the AEGIS survey and CFHTLSD. X-ray images of this field were taken with Chandra as part of the AEGIS-X (Laird et al. 2009). Deep HST images of the EGS were obtained with the Advanced Camera for Surveys (ACS) as part of GO program 10134 (PI: M. Davis). As a part of NMBS-II, this field was imaged in medium-bandwidth filters ($J_1J_2J_3H_1H_2$), and in the K-band. CFHTLS-D3 previously had 20% IRAC data coverage from S-CANDELS, (Ashby et al. 2015).

- CFHTLS-D4 is a 1 deg^2 field centered on RA= 22:15:31.00 and DEC= -17:43:56.00. This field was imaged by CFHT as part of CFHTLS. As a part of NMBS-II, this field was imaged in medium-bandwidth filters ($J_1J_2J_3H_1H_2$), and in the K-band. CFHTLS-D4 had no IRAC coverage previous to this paper.

- MUSYC Extended CDFS (MUSYC-ECDFS) is a 0.5 deg^2 field centered on RA= 03:32:29.0 and DEC= -27:48:47.00. This is one of the fields of the Great Observatories Origins Deep Survey (GOODS; Dickinson & GOODS Legacy Team 2001). Within GOODS, the ACS camera on HST acquired imaging of the ECDFS field. Ground-based optical imaging of the ECDFS with the Wide Field Imager (WFI) on the ESO/MPG 2.2m telescope was obtained as part of the COMBO-17 (Wolf et al. 2004). NIR images of this field were also taken with the VLT/ISAAC. This field has also NIR images in YJHK taken as part of VIDEO survey (Jarvis et al. 2013). As a part of NMBS-II this field was imaged in medium-bandwidth filters ($J_1J_2J_3H_1H_2$), and in the K-band. MUSYC-ECDFS has 100% data coverage from the Spitzer IRAC/MUSYC Public Legacy Survey in the Extended Chandra Deep Field South (SIMPLE, Damen et al. 2011). SIMPLE consists of deep IRAC observations (several hours per pointing) covering the 0.5 x 0.5 deg^2 area surrounding the GOODS CDFS field.

- MUSYC1030 is a 0.5 deg^2 field centered around RA= 10:30:27.10 and DEC= 05:24:55.02. The center of this field is the position of the SDSS quasar SDSS J1030+0524S (Becker et al. 2001). This field was imaged by different telescopes within several surveys. Optical images of this field were taken within the MUSYC survey (Gawiser et al. 2006). Complimentary K-band images were taken using the Infrared Side Port Imager (ISPI) on the 4m Blanco Telescope at the Cerro Tololo Inter-American Observatory (CTIO) in the MUSYC wide NIR survey. As a part of NMBS-II, this field was imaged in medium-bandwidth filters ($J_1J_2J_3H_1H_2$), and in the K-band. MUSYC1030 has 10% IRAC coverage.

- MUSYC1255 is a 0.5 deg^2 centered at RA= 12:55:40.0 and DEC= 01:07:00.00 and also has optical and NIR imaging as part of the MUSYC and MUSYC-NIR surveys. As a part of NMBS-II, this field was imaged in medium-bandwidth filters ($J_1J_2J_3H_1H_2$), and in the K-band. MUSYC1255 has 10% IRAC coverage from the Spitzer Space Telescope Cycle-3 program GO-30873 (PI: Labbe).

2.2. *New IRAC imaging in NMBS-II*

To fully exploit the NMBS-II, in Cycle 10, we were awarded 22 hours on Spitzer to complete the IRAC coverage of the NMBS-II fields in 3.6 μm (3.6μm) and 4.5 μm (4.5μm) (ID:10084; PI: D. Marchesini). The fields imaged in this program were: CFHTLS-D3, CFHTLS-D4,MUSYC1030, andMUSYC1255. The total area mapped in 3.6 μm and 4.5 μm in Cycle 10 is $\sim$ 2.2 deg^2, for a total of 342 individual pointings.
In this paper, we present scientific mosaics and coverage maps for CFHTLS-D1, CFHTLS-D3, CFHTLS-D4,MUSYC1030, andMUSYC1255.

3. DATA REDUCTION

We downloaded all archival data from the Spitzer Heritage Archive (SHA) and combined them with our data sets. We reduced all data in a consistent manner, coadding them into one mosaic per field. We followed the procedure described in (Labbé et al. 2015). The individual exposures are organized into self-contained segments known as Astronomical Observing Requests (AORs). Over the five fields, there are 755 AORs for each filter. Each AOR consists of basic calibrated data (BCD). BCDs are exposure-level data after having passed through the pipelines. Instrumental signatures have been mostly removed, and the BCDs have been absolutely calibrated into physical units (i.e., $MJy/sr = 10^{-17} ergs^{-1} cm^{-2} Hz^{-1} sr^{-1}$). The BCDs were improved by applying a series of procedures in order to remove cosmic rays and remaining instrumental artifacts including column pulldown, muxbleed, maxstripe, and the "first-frame effect" (Hora et al. 2004). Single background-subtracted frames were then combined into a mosaic image large enough to hold all input frames (using WCS astrometry to align the images). In this step, we masked bad pixels

and applied a distortion correction in WCS. This image, in combination with the reference image, was then used to refine the pointing of the individual mosaics. The individual pointing-refined frames were registered to and projected on the reference image.

The reference images for the CFHTLSD-1, CFHTLSD-3, CFHTLSD-4 fields are the $z-$band stack from CFHTLSDeep taken from the CFHTLS T0007 release. These stacks are the combinations of the 25% best seeing images (seeing < 0.95″) of each fields in the $z-$band. Each stack comprises all images located inside a radius of 3′ with respect to a tile center position, weighted accordingly, and combined using SWarp, with a Lanczos3 interpolation kernel. The total exposure times for each of the reference images is 14.20hr, 12.51hr and 12.00 hr, while the seeing is 0.559″, 0.537 ″, and 0.551″, for CFHTLS-D1, CHFTLS-D3, and CFHTLS-D4 respectively. The pixel scale is 0.186 ″/*pixel*. These images are available on the Terapix database (http://terapix.iap.fr/cplt/T0007/table_syn_T0007.html).

The final IRAC mosaics and coverage maps are then resampled to a higher pixel scale value which is listed in Table 1. The reference images for MUSYC1030 and MUSYC1255 are taken with the Infrared Sideport Imager (ISPI) camera mounted at the prime focus of the Blanco 4-m telescope at CTIO in the K-band filter. The original detector pixel scale is 0.305″/pixel. However both K-band images have been previously processed so that the pixel scale is changed slightly to 0.267 and 0.269 ″/pixel, respectively for MUSYC1030 and MUSYC1255. Table 1 summarizes the characteristics of the IRAC data over the five observed fields, such as the total exposure time, the number of AORs that contributed to the mosaic, and the pixel scale at 3.5 μm and 4.5 μm. For comparison, we also add, where available, the characteristics of the other two fields.

In Figures 1, 2, 3, 4, and 5, we show the reference image, the two IRAC mosaics at 3.6 μm and 4.5 μm and the corresponding coverage maps for each of the five fields.

4. MOSAIC QUALITY

In this section, we describe the quality of the final mosaics in both channels for each of the five NMBS-II fields.

To characterize the FWHM and the PSF of these mosaics we proceed in this way. First, we define a sample of ∼ 50 bright, isolated and unsaturated stars in each channel and each field. Then, for each star in the sample we measured a curve of growth, i.e. the distribution of the light at different radii, normalized by the flux of the star in aperture of sufficiently large diameter (6″). For each field, we consider the median of this growth curves in each channel (black curves in Fig. 6 and Fig. 7). Outliers, such as saturated stars, were then determined based on the shape of their light profile compared with the median curve of growth, and rejected from the sample. We use the median growth curve in each field to derive the median half-light and 75%-light radii, i.e., the radii that contain 50% and 75% of the light, respectively. These values are reported in Table 2. The same sample of stars is also used to derive the FWHMs of the IRAC images. The derived FWHM are listed in Table 2. We stress that the IRAC PSF is complicated and that spatial variations across the field of view are to be expected given we mosaiced IRAC data taken from several independent programs. However, the state-of-the-art approach to extract IRAC photometry from wide and deep surveys consists in the adoption of software that accounts for spatially varying PSF across the field of view, such as MOPHONGO (Labbé et al. 2006), TFIT (Laidler et al. 2007), and T-PHOT (Merlin et al. 2015).

In Table 3, we list the 3σ magnitude depth for all mosaics. For comparison, we also add, where available, the FWHMs and 3σ magnitude depths of the other two fields taken from the literature papers mentioned in Sect. 2.

We use the "empty aperture" method to empirically determine the noise properties of our IRAC mosaics, following the same approach as for the deep NIR MUSYC data (Quadri et al. 2007). Briefly, we randomly place a large number of apertures on the noise-normalized images (obtained by multiplying the images by the square root of the coverage maps), reject all apertures falling on sources, and measure the flux in the remaining ones. We chose an aperture size of 3″ and measure the flux in ∼ 8000 apertures for CFHTLSD fields and ∼ 4000 in the MUSYC fields. A histogram of the measured fluxes is constructed for each field in both 3.6 μm and 4.5 μm, and shown in Figures 8, 9, 10, 11 and 12 (bottom panels). These histograms are all well fitted by a Gaussian. The top panels of Figures 8, 9, 10, 11 and 12 show the maps of 3σ magnitude depths derived using the empty aperture method according to the Equation:

$$\mathrm{depth}(3\sigma)[\mathrm{AB}] = -2.5\log\left(\frac{3\sigma_{\mathrm{best-fit}}}{\sqrt{\mathrm{COVERAGE\,MAP}}}\right) + \mathrm{ZP}, \quad (1)$$

where ZP is listed in Table 1 for each field. Table 3 lists the 15th, 50th, and 75th percentiles of the 3σ magnitude depths in both 3.6 μm and 4.5 μm in an aperture of D=3″ as derived with the empty aperture method. The median value of the 3σ depths for 3.6 μm varies from 22.83 mag (in CFHTLSD4) to 24.52 (in CFHTLSD1), while for 4.5 μm it varies from 22.85 mag (in CFHTLSD4) to 24.44 (in CFHTLSD1). As expected, regions with higher exposure times (see Figures 1, 2, 3, 4, and 5) also have fainter 3σ magnitude depths. As shown in Figure 9, using both the images observed in this program and the data collected by the AEGIS survey, we present results in an extremely deep mosaic in some of the

Table 1. Characteristics of the IRAC observations

Filter (μm)	PIDs[a]	Max Exposure Time[b] (h)	Number of AORs	Pixel scale (arcsec/pixel)	ZP (AB)
CFHTLS-D1:					
3.6	181	8.18	262	0.558	20.04
4.5	181	7.31	262	0.558	20.04
CFHTLS-D2[c]:					
3.6	20070, 61043,80057, 90042, 10159, 11016			0.6	
4.5	20070, 61043,80057, 90042, 10159, 11016			0.6	
CFHTLS-D3:					
3.6	8, 41023, 61042, 80216, 10084	29.3	456	0.558	20.04
4.5	8, 41023, 61042, 80216, 10084	26.8	456	0.558	20.04
CFHTLS-D4:					
3.6	10084	1.32	13	0.558	20.04
4.5	10084	0.89	13	0.558	20.04
MUSYC-ECDF[d]:					
3.6	20708	2.5		0.6	22.42
4.5	20708	2.5		0.6	22.19
MUSYC1030:					
3.6	3198, 10084	1.70	11	0.267	20.04
4.5	3198, 10084	1.76	11	0.267	20.04
MUSYC1255:					
3.6	30873, 10084	1.40	13	0.269	20.04
4.5	30873, 10084	1.46	13	0.269	20.04

[a] Spitzer Program Identification Numbers

[b] Maximum exposure time per position on sky per channel.

[c] The characteristics of this field are taken from Ashby et al. 2018

[d] The characteristics of this field are taken from Damen et al. 2011

regions of CFHTLSD3.

5. PUBLIC DATA RELEASE

The data release consists of reduced images of all IRAC observations in three CFHTLSD fields, namely CFHTLS-D1, CFHTLS-D3, CFHTLS-D4, and two MUSYC fields, MUSYC1030, and MUSYC1255. The images are available on the website: `http://cosmos.phy.tufts.edu/~danilo/NMBS2irac`. The data release contains the following:

- Mosaic science images in both 3.6 μm and 4.5 μm. The images are W-registered to the reference image. This reference image is either the z-band stack image of the 25% best seeing images from the CFHTLSDeep for CFHTLS-D1, CFHTLS-D3, CFHTLS-D4, or the K-band images obtained at the Blanco 4-m telescope at CTIO for MUSYC1030 and MUSYC1255.
- Coverage maps containing exposure times (seconds) in both 3.6 μm and 4.5 μm.
- Maps with 3σ magnitude depth (as derived in Section 4) at the same WCS and pixel scales of the scientific images.

ACKNOWLEDGMENT

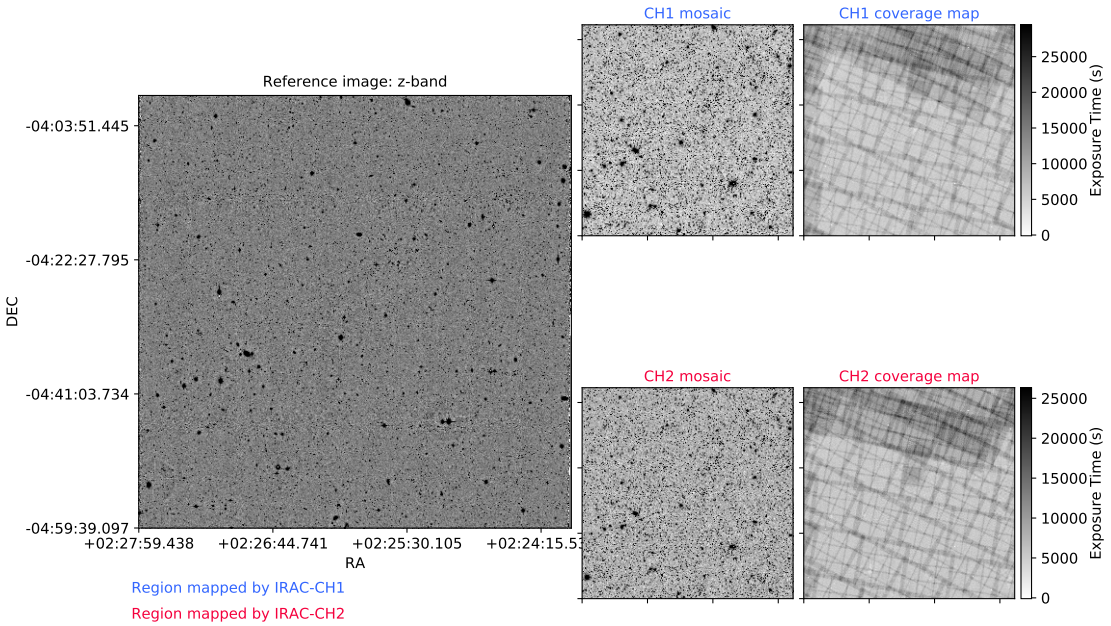


Figure 1. CFHTLS-D1: reference band mosaic, 3.6μm and 4.5μm mosaics and coverage maps. The coverage maps show where the individual pointings of IRAC overlap when they are combined to form the mosaic. Pixels with darker colors have more coverage.

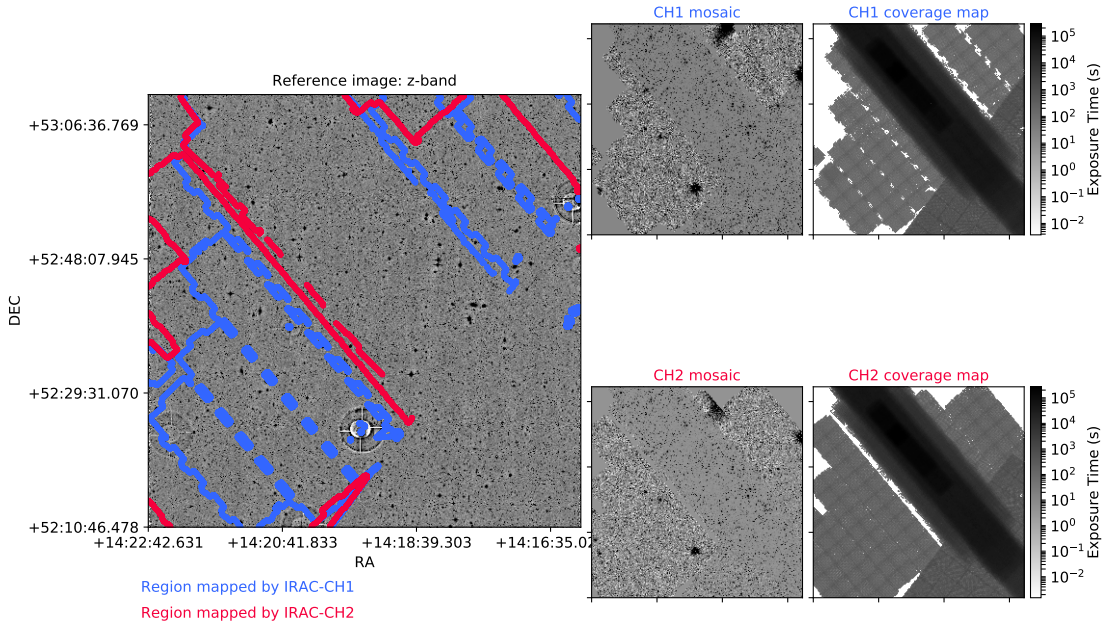


Figure 2. Same as in Figure 1, but for the CFHTLS-D3 field. For this field, we use a logarithmic scale for the coverage maps to show simultaneously the regions with the highest and lowest coverage.

The reduction and public release of the Spitzer-IRAC data in the NEWFIRM Medium-Band Survey II was supported by the National Aeronautics and Space Administration (NASA) under award number NNX16AN49G issued through the NNH15ZDA001N Astrophysics Data Analysis Program (ADAP). The Cosmic Dawn Center is funded by the Danish National Research Foundation. We thank the anonymous referee for his/her useful comments.

REFERENCES

Ashby, M. L. N., Caputi, K. I., Cowley, W., et al. 2018, ArXiv e-prints

Ashby, M. L. N., Willner, S. P., Fazio, G. G., et al. 2015, ApJS, 218, 33

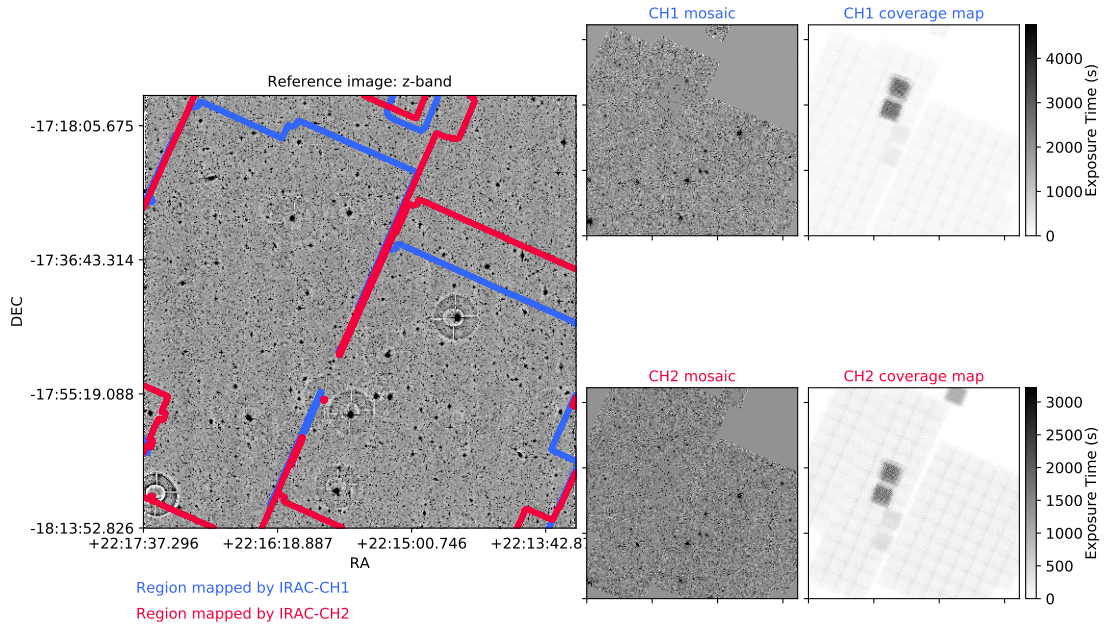


Figure 3. Same as in Figure 1, but for the CFHTLS-D4 field.

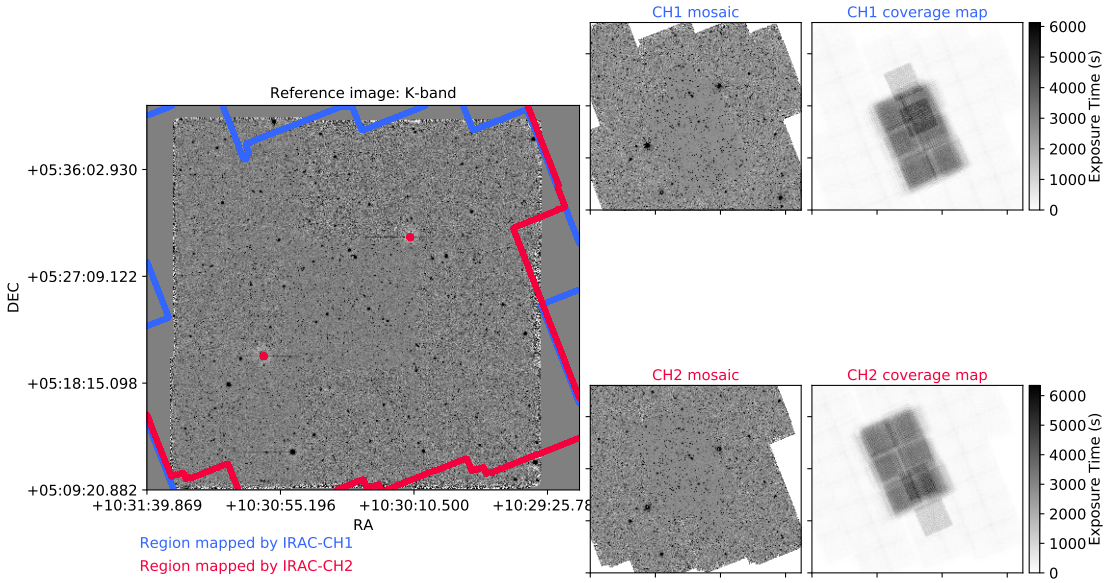


Figure 4. Same as in Figure 1, but for the MUSYC1030 field.

Ashby, M. L. N., Willner, S. P., Fazio, G. G., et al. 2013, ApJ, 769, 80

Becker, R. H., Fan, X., White, R. L., et al. 2001, AJ, 122, 2850

Bielby, R., Hudelot, P., McCracken, H. J., et al. 2012, A&A, 545, A23

Brammer, G. B., Whitaker, K. E., van Dokkum, P. G., et al. 2009, ApJL, 706, L173

Chiappetti, L., Tajer, M., Trinchieri, G., et al. 2005, A&A, 439, 413

Damen, M., Labbé, I., van Dokkum, P. G., et al. 2011, ApJ, 727, 1

Davis, M., Guhathakurta, P., Konidaris, N. P., et al. 2007, ApJL, 660, L1

Dekel, A., Birnboim, Y., Engel, G., et al. 2009, Nature, 457, 451

Dickinson, M. & GOODS Legacy Team. 2001, in Bulletin of the American Astronomical Society, Vol. 33, American Astronomical Society Meeting Abstracts #198, 820

Elvis, M., Civano, F., Vignali, C., et al. 2009, ApJS, 184, 158

Fazio, G. G., Hora, J. L., Allen, L. E., et al. 2004, ApJS, 154, 10

Finoguenov, A., Guzzo, L., Hasinger, G., et al. 2007, ApJS, 172, 182

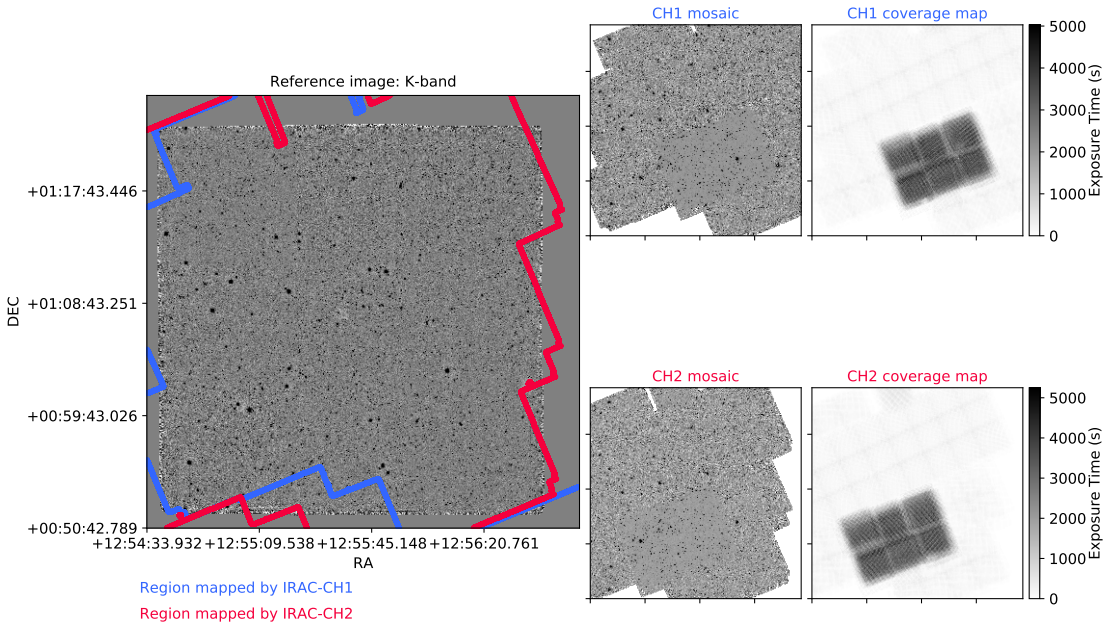


Figure 5. Same as in Figure 1, but for the MUSYC1255 field.

Fontanot, F., De Lucia, G., Monaco, P., Somerville, R. S., & Santini, P. 2009, MNRAS, 397, 1776

Gawiser, E., van Dokkum, P. G., Herrera, D., et al. 2006, ApJS, 162, 1

Griffin, M. J., Abergel, A., Abreu, A., et al. 2010, A&A, 518, L3

Hirschmann, M., De Lucia, G., & Fontanot, F. 2016, MNRAS, 461, 1760

Hopkins, P. F., Hernquist, L., Cox, T. J., et al. 2006, ApJS, 163, 1

Hora, J. L., Latter, W. B., Allen, L. E., et al. 2004, ApJS, 154, 296

Ilbert, O., McCracken, H. J., Le Fèvre, O., et al. 2013, A&A, 556, A55

Jansen, F., Lumb, D., Altieri, B., et al. 2001, A&A, 365, L1

Jarvis, M. J., Bonfield, D. G., Bruce, V. A., et al. 2013, MNRAS, 428, 1281

Koekemoer, A. M., Faber, S. M., Ferguson, H. C., et al. 2011, ApJS, 197, 36

Labbé, I., Bouwens, R., Illingworth, G. D., & Franx, M. 2006, ApJL, 649, L67

Labbé, I., Oesch, P. A., Illingworth, G. D., et al. 2015, ApJS, 221, 23

Laidler, V. G., Papovich, C., Grogin, N. A., et al. 2007, PASP, 119, 1325

Laird, E. S., Nandra, K., Georgakakis, A., et al. 2009, ApJS, 180, 102

Le Fèvre, O., Tasca, L. A. M., Cassata, P., et al. 2015, A&A, 576, A79

Lilly, S. J., Le Fèvre, O., Renzini, A., et al. 2007, ApJS, 172, 70

Lonsdale, C. J., Smith, H. E., Rowan-Robinson, M., et al. 2003, PASP, 115, 897

Marchesini, D., van Dokkum, P. G., Förster Schreiber, N. M., et al. 2009, ApJ, 701, 1765

Marchesini, D., Whitaker, K. E., Brammer, G., et al. 2010, ApJ, 725, 1277

McCracken, H. J., Milvang-Jensen, B., Dunlop, J., et al. 2013, The Messenger, 154, 29

Merlin, E., Fontana, A., Ferguson, H. C., et al. 2015, A&A, 582, A15

Muzzin, A., Marchesini, D., Stefanon, M., et al. 2013a, ApJ, 777, 18

Muzzin, A., Marchesini, D., Stefanon, M., et al. 2013b, ApJS, 206, 8

Oliver, S. J., Bock, J., Altieri, B., et al. 2012, MNRAS, 424, 1614

Pilbratt, G. L., Riedinger, J. R., Passvogel, T., et al. 2010, A&A, 518, L1

Quadri, R., Marchesini, D., van Dokkum, P., et al. 2007, AJ, 134, 1103

Sanders, D. B., Salvato, M., Aussel, H., et al. 2007, ApJS, 172, 86

Scoville, N., Aussel, H., Benson, A., et al. 2007, ApJS, 172, 150

Somerville, R. S., Hopkins, P. F., Cox, T. J., Robertson, B. E., & Hernquist, L. 2008, MNRAS, 391, 481

Steinhardt, C. L., Speagle, J. S., Capak, P., et al. 2014, ApJ, 791, L25

Tanaka, M., Hasinger, G., Silverman, J. D., et al. 2017, ArXiv e-prints

Taniguchi, Y., Kajisawa, M., Kobayashi, M. A. R., et al. 2015, PASJ, 67, 104

van Dokkum, P. G., Brammer, G., Fumagalli, M., et al. 2011, ApJL, 743, L15

Werner, M. W., Roellig, T. L., Low, F. J., et al. 2004, ApJS, 154, 1

Table 2. Characteristics of the IRAC observations

Filter (μm)	FWHM ($''$)	50% light radius ($''$)	75% light radius ($''$)
CFHTLS-D1:			
3.6	2.08	2.20	3.28
4.5	1.95	2.20	3.39
CFHTLS-D2[a]:			
3.6	~ 2.00		
4.5	~ 2.00		
CFHTLS-D3:			
3.6	2.00	2.15	3.22
4.5	1.86	2.16	3.38
CFHTLS-D4:			
3.6	1.86	2.08	3.17
4.5	1.75	2.14	3.35
MUSYC-ECDF[b]:			
3.6	1.97		
4.5	1.93		
MUSYC1030:			
3.6	2.17	2.11	3.18
4.5	2.01	2.16	3.35
MUSYC1255:			
3.6	2.02	2.09	3.17
4.5	1.98	2.11	3.34

[a] The FWHM of this field are taken from Ashby et al. 2018.

[b] The FWHM of this field are taken from Damen et al. 2011.

Whitaker, K. E., Labbé, I., van Dokkum, P. G., et al. 2011, ApJ, 735, 86

Wolf, C., Meisenheimer, K., Kleinheinrich, M., et al. 2004, A&A, 421, 913

Table 3. Depths of the IRAC observations

Filter (μm)	15th percentile of 3σ depth[a] (AB)	Median of 3σ depth [a] (AB)	75th percentile of 3σ depth[a] (AB)
CFHTLS-D1:			
3.6	24.33	24.52	24.66
4.5	24.24	24.44	24.58
CFHTLS-D2[b]:			
3.6		25.31	
4.5		25.31	
CFHTLS-D3:			
3.6	22.79	23.76	25.54
4.5	22.88	23.45	25.29
CFHTLS-D4:			
3.6	22.53	22.83	23.00
4.5	22.51	22.85	23.03
MUSYC-ECDF[c]:			
3.6	24.21	24.41	24.55
4.5	24.05	24.24	24.37
MUSYC1030:			
3.6	22.63	22.92	23.20
4.5	22.63	22.97	23.24
MUSYC1255:			
3.6	22.60	22.87	23.10
4.5	22.44	22.75	23.00

[a] Using a 3″ circular aperture diameter.

[b] The 3σ depths of this field are taken from Ashby et al. 2018.

[c] The 3σ depths of this field are taken from Damen et al. 2011.

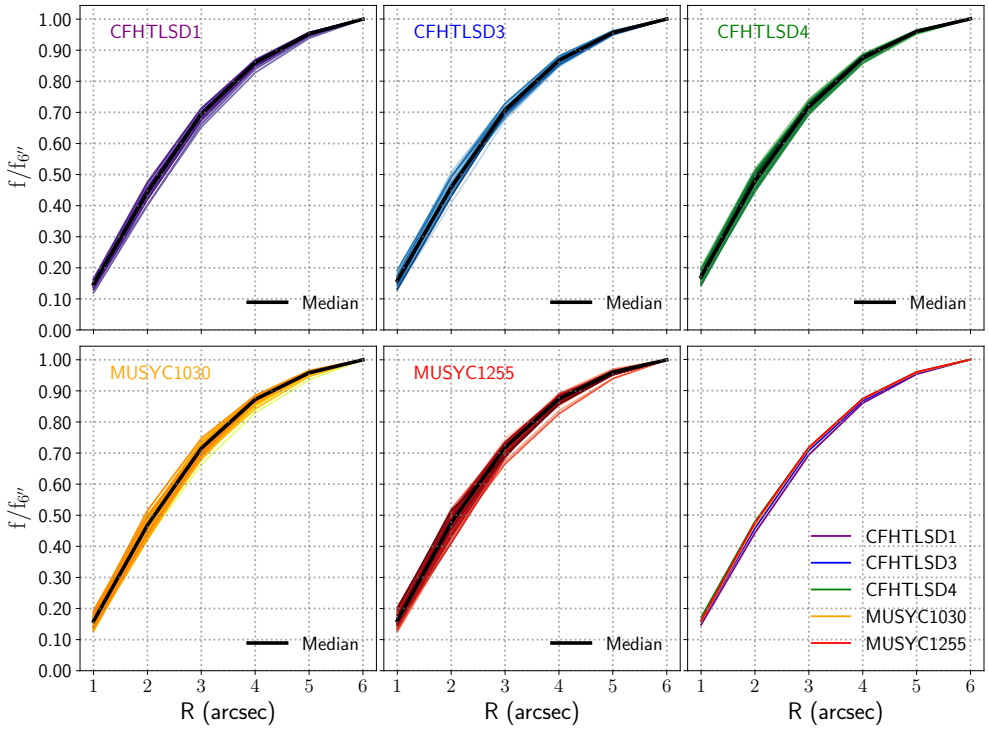


Figure 6. First five panels: Growth curves for a sample of ∼ 50 bright unsaturated stars for all five fields at 3.6μm normalized to the flux of the star in an aperture of 6″ diameter. The black curve in each panel represents the median of the distribution. The bottom-right panel shows the median growth curve of each field at 3.6μm.

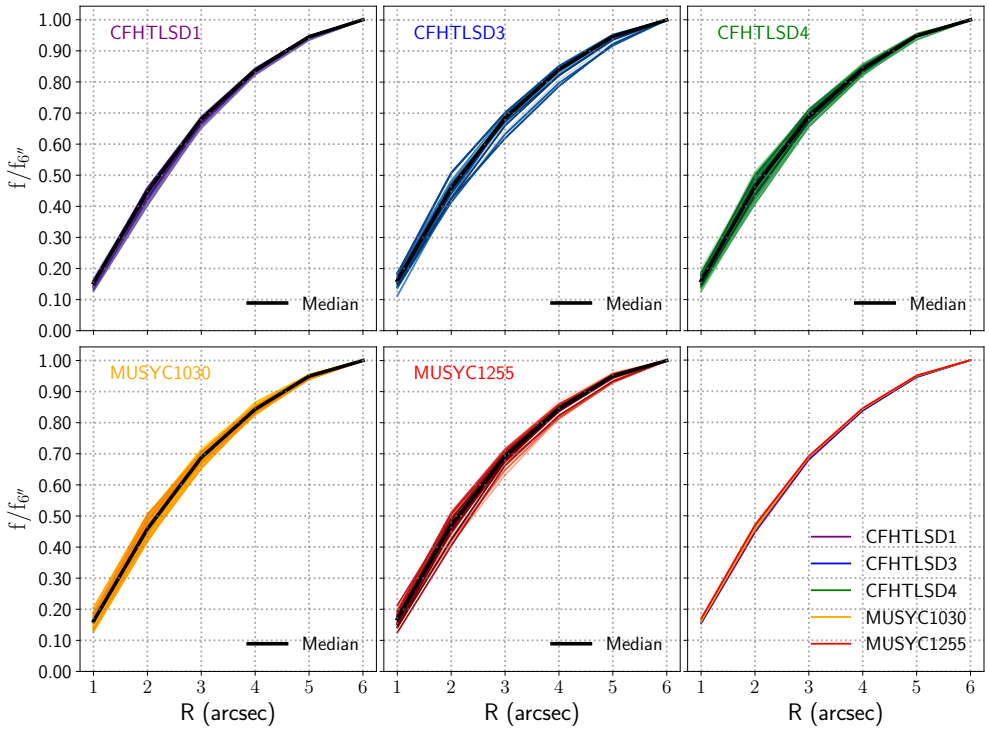


Figure 7. Same as in Fig. 6, but at 4.5μm.

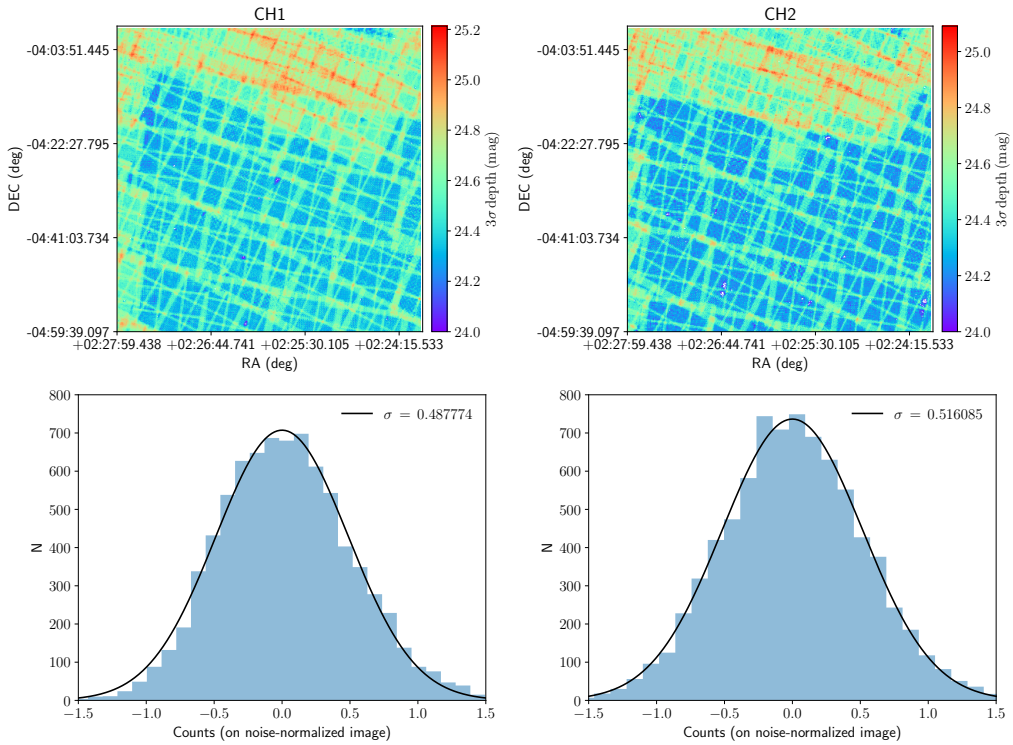


Figure 8. CFHTLSD1: Top row: 3σ magnitude depths of 3.6 μm and 4.5 μm mosaics. Bottom row: Histograms of enclosed fluxes measured on ~ 8000 empty apertures in 3.6 μm and 4.5 μm on the noise-normalized images. Best-fit Gaussians are also shown.

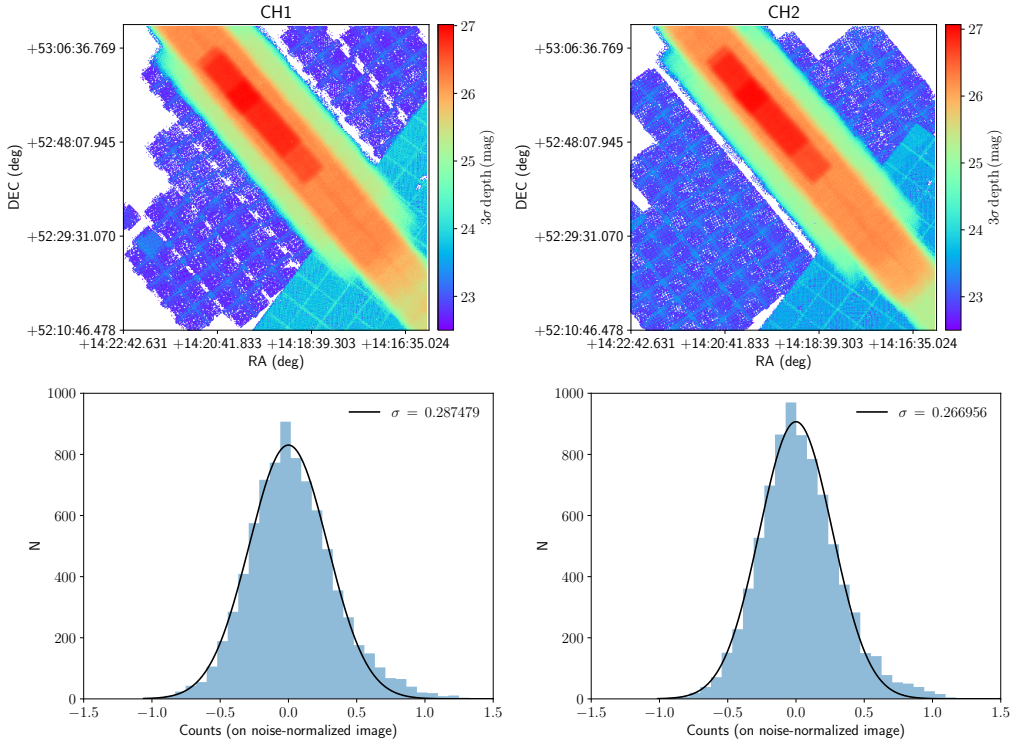


Figure 9. Same as in Figure 8, but for the CFHTLS-D3 field.

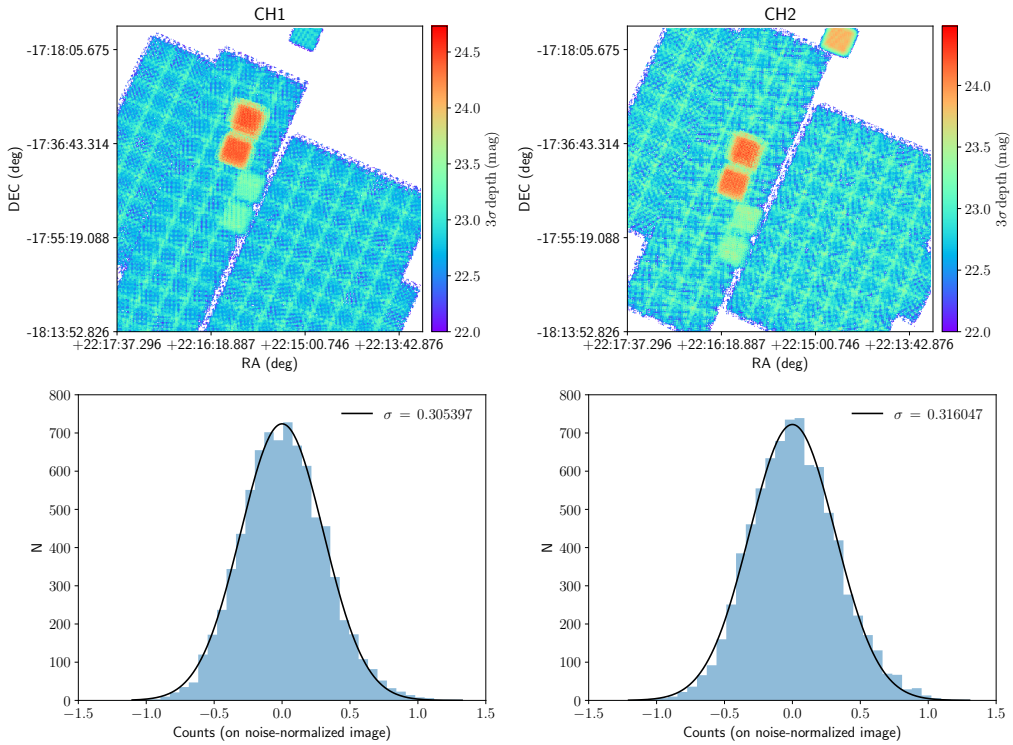


Figure 10. Same as in Figure 8, but for the CFHTLS-D4 field.

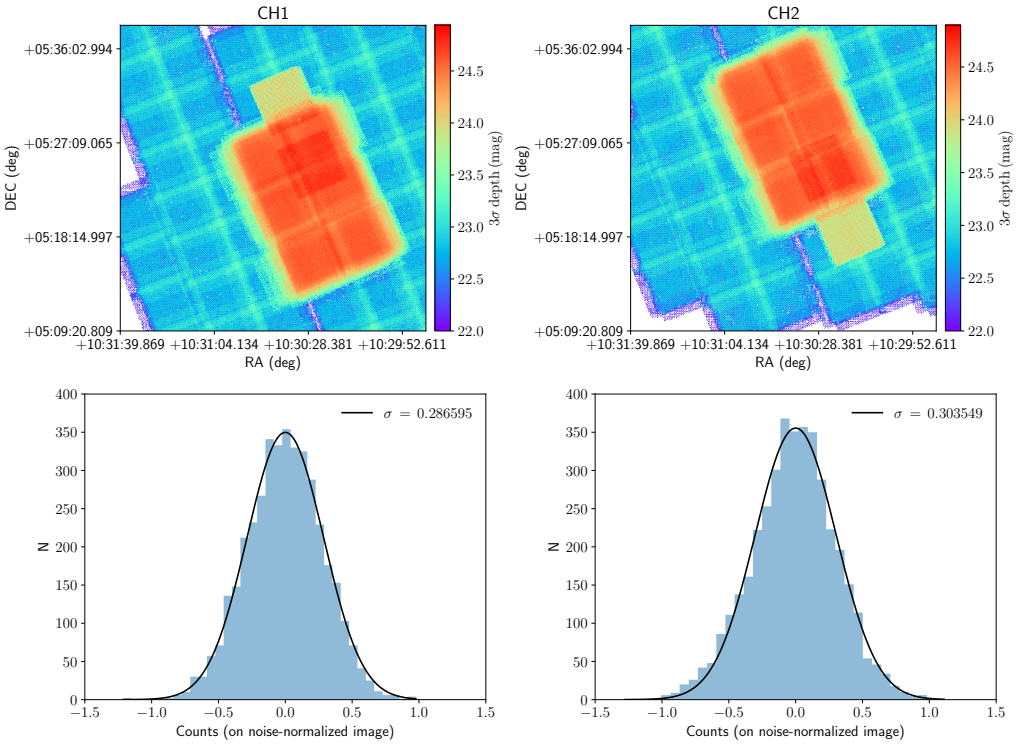


Figure 11. MUSYC1030: Top row: 3σ magnitude depths of 3.6 μm and 4.5 μm mosaics. Bottom row: Histograms of enclosed fluxes measured on $\sim$ 4000 empty apertures in 3.6 μm and 4.5 μm on the noise-normalized images. Best-fit Gaussians are also shown.

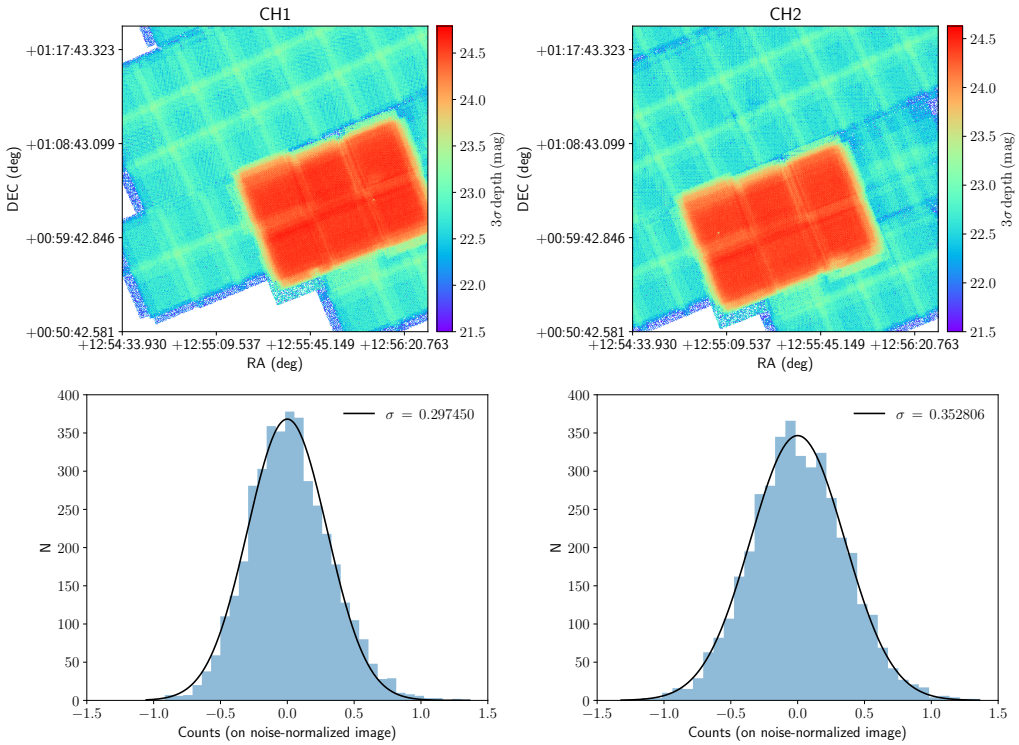


Figure 12. Same as in Figure 11, but for the MUSYC1255 field.